Preparation of size-controlled nanoparticles of magnetite

Ângela L. Andrade [a,b,*], Manuel A. Valente [c], José M.F. Ferreira [a], José D. Fabris [d]

[a] Department of Ceramics and Glass Engineering, CICECO, University of Aveiro, Aveiro P-3810193, Portugal
[b] Department of Chemistry, Federal University of Ouro Preto, 35400-000 Ouro Preto, Minas Gerais, Brazil
[c] Department of Physics, I3N, University of Aveiro, Aveiro P-3810193, Portugal
[d] Federal University of Jequitinhonha and Mucuri Valleys (UFVJM), 39100-000 Diamantina, Minas Gerais, Brazil

ABSTRACT

Samples of ferrofluids containing chemically stabilized nanoparticles of magnetite (Fe_3O_4) with tetramethylammonium hydroxide (TMAOH) were prepared by a direct reduction–precipitation method. The influences of aging time and temperature on the size and monodispersion characteristics of the produced nanoparticles were investigated. Transmission electron microscopy, powder X-ray diffraction, Fourier-transform infrared, and magnetization measurements with applied magnetic field up to 2 T were used to characterize the synthesized iron oxides. Raising the temperature of the synthesized material in autoclave affects positively the monodispersion of the nanoparticles, but it was not found to significantly influence the size itself of individual particles.

© 2011 Elsevier B.V. Open access under the Elsevier OA license.

1. Introduction

Magnetic nanoparticles have been drawing expressive technological interests for their outstanding properties and potential applications in various fields, including ferrofluids materials, catalysts, colored pigments, high-density magnetic recording media, and medical diagnostics and therapy [1–5]. The size and morphology of nanoparticles are two important characteristics influencing their electrical, optical, and magnetic properties [6–9]. The way nanoparticles are synthesized may determine their morphological uniformity and size distribution; these conditions become one of the key challenging issues in nanoscience and nanotechnology [10,11]. More recently, mixed and pharmacologically coated magnetic nanoparticles have been suitably prepared in order to be used in biological applications and in medical diagnoses and therapy in oncology. Some applications associated with superparamagnetic nanoparticles are cellular therapy such as labeling and targeting in cell-biology practices as to separate and purify cell populations, tissue repair, drug delivery, magnetic resonance imagery (MRI), hyperthermia, and magnetofection [12–15].

Syntheses of nanoparticles with variable sizes and size or homogeneous morphology have been intensively tried particularly for magnetic iron oxides with spinel structure, namely maghemite (γFe_2O_3) and magnetite (Fe_3O_4). However complex preparation processes may be required to assure sorting out particles with designed size and morphology [16–19]. Most commonly, Fe_3O_4 nanoparticles are prepared *via* coprecipitating ferrous and ferric ions in aqueous solution [20,21]. However, the corresponding chemical reactions do occur very fast, just promptly on mixing reactants, and this makes it very difficult to control the crystallization process. As a consequence, the magnetic nanoparticles of the resulting iron oxides tend to exhibit relatively poor size uniformity and crystallinity, and this feature may limit their use in many technological applications.

The solvothermal process is one of the successful methods to grow crystals, in which the formed magnetite grains have much higher crystallinity than those prepared from other methods. However, the chemical composition of the starting organometalic compounds used in this synthesis limits further several applications, taking into account the (a) hazardous nature of precursors; (b) complex manipulation of chemicals and conditions during synthesis; (c) high cost of the materials needed, and (d) low chemical yields of products [22].

The present work aimed at proposing a relatively simpler preparation of size-controlled superparamagnetic iron oxides nanoparticles through a reduction–precipitation method combined with a thermal treatment. The produced magnetic samples were mildly heated to 50 °C and 100 °C for 1 h, 3 h, and 5 h, in a procedure intended to clean them up from surface water or chemical reactants and increase their structural stability, preventing from any easily oxidation of the nano-grained magnetite. In this procedure, instead of using the usually toxic and expensive organometallic compound as precursors, it is proposed a new method to synthesize monodispersed magnetite nanocrystals,

* Corresponding author at: Federal University of Ouro Preto, Department of Chemistry, 35400-000 Ouro Preto, Minas Gerais, Brazil.
E-mail address: angelaleao@iceb.ufop.br (A.L. Andrade).

with higher product yields than through most of the conventional methods. To ensure that the Fe_3O_4 nanoparticles are monodispersed, their surfaces were modified by adsorbing tetramethylammonium hydroxide (TMAOH), in order to prevent their agglomeration in aqueous solution, as they are required, for instance, to be better suitable for using in medical diagnosis and therapeutic practices.

2. Experimental

2.1. Materials and reagents

All chemicals used in this work, namely $FeCl_3 \cdot 6H_2O$ (Riedel-de Haen), HCl (Fluka), Na_2SO_3 (Sigma-Aldrich), ammonium hydroxide (Fluka), and 25% aqueous tetramethylammonium hydroxide solution (TMAOH) (Sigma-Aldrich), were of analytical grade standards and used as received.

2.2. Iron oxide nanoparticles preparation

The synthesis procedure used to prepare these magnetite samples was described in details in Ref. [23]. It was based on the method earlier proposed by Qu et al. [24], and essentially consisted in adding 20 mL of 1 mol L^{-1} Na_2SO_3 to 30 mL of 2 mol L^{-1} $FeCl_3 \cdot 6H_2O$, in a medium previously acidified with HCl, into a 1000 mL 3-necked round bottom flask, while bubbling-in N_2 gas, in order to assure as much as possible a chemically inert atmosphere. The suspension containing the precipitated powder was centrifuged at 2000 rpm for 3 min; the supernatant was discarded. This procedure was repeated five times by re-dispersing the resultant cakes in distilled water. The as obtained precipitate was labeled Mt. The nanoparticles were then treated so to be coated with tetramethylammonium hydroxide (TMAOH). Typically, 1 mL of commercial 25% TMAOH solution was added to each centrifuge tube containing an amount of wet cake corresponding to about 1 g dry powder and re-dispersed with a thin glass rod until obtaining homogeneous suspensions. These suspensions were then dried to obtain the final powders. The sample that was treated with TMAOH in order to obtain the surface coated nanoparticles was labeled Mt1.

TMAOH was used as protective agent to decrease particle aggregation, due interparticle interaction; the electrostatic repulsion effect is mainly caused by charges of the tetramethylammonium cations adsorbed on the particle surface, in the water medium. The obtained mixture was sealed in a teflon-lined stainless-steel autoclave of 50 mL capacity, and heated at 50 °C or 100 °C. The so assembled system was kept at the selected temperature in an oven for 1 h, 3 h, or 5 h and allowed for spontaneously cooling down to room temperature. The resulting products were separated with a permanent magnet, washed out with distilled water and acetone, and dried at room temperature. Magnetic particles were picked-up from the aqueous suspension, with a small hand magnet. The magnetization of iron-rich spinels tends to decrease as particle sizes become smaller. The effectiveness of this separation in this case was rather limited not only due to small sizes of the magnetic particles but also to the low strength of the magnetic field generated by the small hand magnet. In view of these main effects most particles actually remained in suspension after magnetic separation. The samples autoclave-heated at 50 °C for 1 h, 3 h, and 5 h were labeled Mt1-51, Mt1-53, and Mt1-55, respectively; those heated at 100 °C for 1 h, 3 h, and 5 h were labeled Mt1-101, Mt1-103, and Mt1-105, respectively. The heating time and the temperature were chosen in an attempt to control the size and monodispersity of the produced nanoparticles.

2.3. Characterization

The size and morphology of the synthesized particles were determined by directly measuring their dimensions on images obtained with a Hitachi, 9000 NA (Japan) transmission electron microscope (TEM), using a drop of the sample suspension onto a copper mesh coated with an amorphous carbon film. This mesh was then dried in a vacuumed desiccator. Any attempts to improve dispersing agglomerated particles in the suspension with a low-power ultra-sound bath were virtually unsuccessful. The crystalline structure of the magnetic nanoparticles, after evaporating the liquid carrier of samples, were assessed with powder X-ray diffraction (XRD) measurements, using a Rigaku Geigerflex D/Max, C Series and $Cu(K\alpha)$ radiation, with 2θ angles ranging from 25° to 70° by steps of 0.02°/s. The crystalline phases were identified by comparing the experimental X-ray patterns with standard data from files of the International Center for Diffraction Data. The ATR-FTIR data were collected with a FT-IR model Mattson Galaxy S-7000, 32 scans, and resolution of 4 cm^{-1}.

The magnetization curves were obtained with 100 to 150 mg of each sample in a vibrating sample magnetometer (VSM) with a cryogen free magnet (Cryogenic–Cryofree) at the University of Aveiro, Portugal. Typical hysteresis curves were obtained at 300 ± 0.1 K, and with a magnetic field between -2 and 2 T. The magnetic parameters, specifically saturation magnetization (M_s), magnetic coercivity (H_c) and remanence (M_r) were deduced from these VSM results.

3. Results and discussion

Colors of iron oxide may be very dependent on grain size and chemical composition and this feature is a first auxiliary attribute in their identification, and may even be eventually used as a rule of thumb guide to purity [25,26]. In this work, all samples are typically black in color and are magnetic, which suggest that magnetite may be the dominant phase, although ancillary maghemite may not be completely excluded.

The size and morphology of particles of these samples, prepared under different reaction conditions, were analyzed with transmission electron microscopy (TEM).

Comparing TEM pictures for samples Mt and Mt1 (Fig. 1) it can be observed that particles in Mt1 are better dispersed than in Mt. This was actually expected, as tetramethylammonium hydroxide (TMAOH) acts as a surface-active agent [25] favoring the dispersion of Fe_3O_4 (magnetite) nanoparticles.

Among the thermally treated samples, the one heated at 50 °C for 1 h showed the most uniformly size-distributed nanoparticles, with only some few observable agglomerates (Fig. 2). Typical TEM image for the sample Mt1-51 (Fig. 2) is presented to serve as an illustration of the typical morphology, and the way the averaged particle sizes of magnetic grains were determined for all samples, from directly measuring individual grains on the complete set of electron-microscopy images (not shown). This result indicates an overall trend for the autoclave-treated materials to form the smallest particles among all of these samples. From TEM original images the thermal treatment does affect both the dispersion and the mean sizes of particles.

In general, particles for all samples were found to be approximately isometric in shape; the thermal treatment tends to narrow their particle size distributions.

Fig. 3 shows X-ray diffraction patterns for all samples. It can be observed that the positions of the characteristic reflection peaks of the spinel structure are consistent with the standard diffraction reflections for magnetite (ICDD card # 88-0866). Taking into account the typically small differences between typical XRD
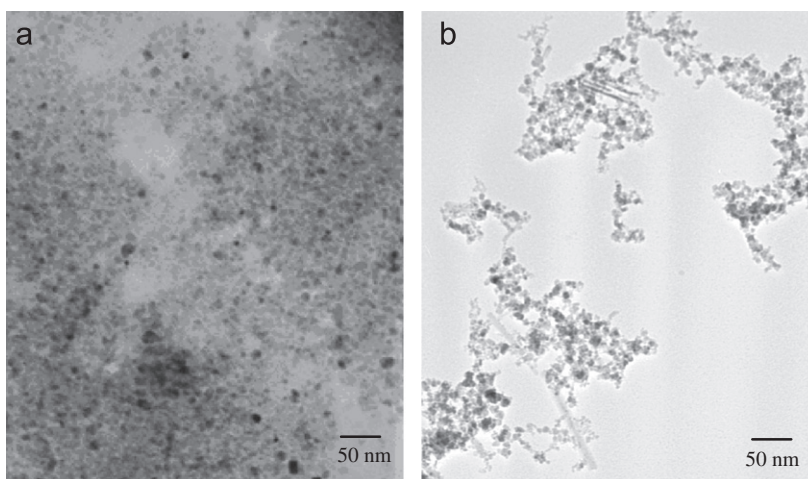
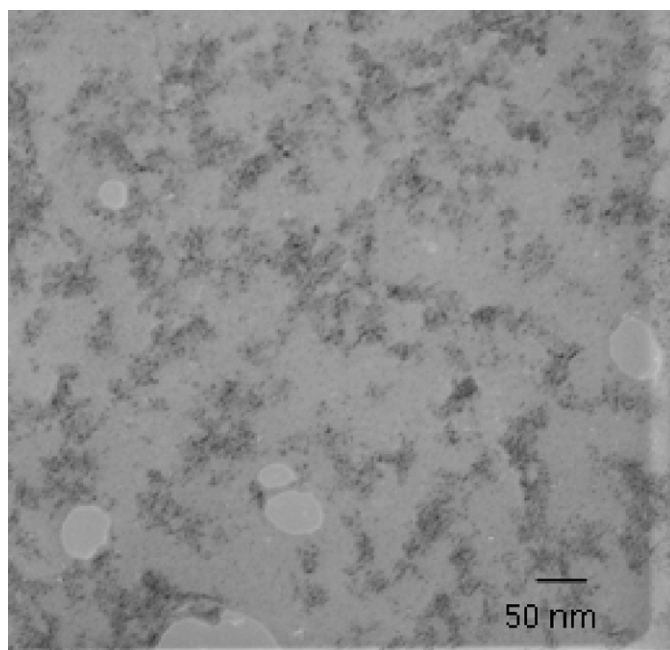**Fig. 1.** TEM micrographs of samples: (a) Mt; (b) Mt1.

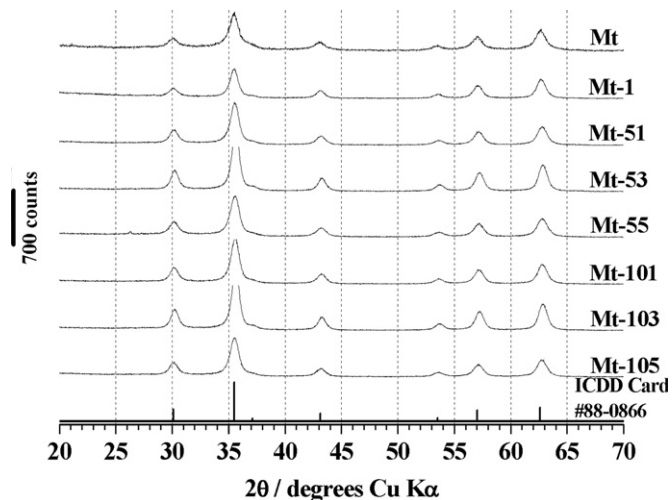**Fig. 2.** TEM micrograph of sample Mt1-51.

Fig. 3. X-ray diffraction patterns of samples: (a) Mt, (b) Mt1-, (c) Mt1-51, (d) Mt1-53, (e) Mt1-55, (f) Mt1-101, (g) Mt1-103, (h) Mt1-105, and (i) magnetic (ICDD File No: 88-0866.).

patterns for magnetite and maghemite, these two phases may be only hardly distinguished in such an intimate mixture. No clear reflection peak due to other crystalline phase, which could occur as impurity, was observed, indicating that final products were pure enough, from this point of view, consisting essentially of a binary mixture of the two spinel magnetic iron oxides, meaning magnetite and maghemite. The intensities of the reflection peaks in these X-ray diffraction patterns for the sample Mt1 are in general smaller than those for the sample Mt. This means that the surface-active agent tends to hinder the growth of the nanoparticles, keeping them in a monodispersed state. The average particle sizes for all samples, from breadths of reflection 311, estimated with Scherrer equation [27] are shown in the Table 1.

ATR-FTIR spectra for these samples are shown in the Fig. 4. The spectrum (Fig. 4) for sample TMAOH shows a strong band at $1490 \, cm^{-1}$ assignable to the asymmetric methyl deformation mode, $\delta_{asym}(CH_3)$. Another single band appears at $950 \, cm^{-1}$, assignable to the asymmetric methyl deformation mode C–N, which is generally observed in the domain 900–$1000 \, cm^{-1}$ [28].

Table 1
Mean coherence lengths (MCL), reflecting changes in particle sizes for samples, as determined with the Scherrer formula. Uncertainty figures were taken as being standard deviations over the mean values estimated from peak breadth measurements for the different reflections spanning the corresponding X-ray diffraction patterns.

Sample	MCL/nm
Mt	11 ± 1
Mt1	6 ± 3
Mt1-51	6 ± 3
Mt1-53	7 ± 3
Mt1-55	5 ± 2
Mt1-101	4 ± 3
Mt1-105	5 ± 3

The ATR-FTIR pattern for the Mt sample (Fig. 4) shows a band at $550 \, cm^{-1}$, which is the characteristic of magnetite [29–31]. Patterns for samples Mt1, Mt1-51, Mt1-53, Mt1-55, Mt1-101, Mt1-103, and Mt1-105 (Fig. 4) show typical bands of TMAOH and of magnetite. The observed bands at 850 and $1070 \, cm^{-1}$ are assignable to CH_2 vibrations [32]. ATR-FTIR bands observed from the spectra for Mt1, Mt1-51, Mt1-53, Mt1-55, Mt1-101, Mt1-103,

and Mt1-105 samples (Fig. 4) evidence that the TMAOH indeed coats the sample gains.

Fig. 5 shows the magnetization curves at 300 K for the just after synthesized and also for the thermally treated powders. The curves indicate a superparamagnetic behavior for all the studied samples, as evidenced by both zero coercivity and zero remanance on the magnetization loop. The measured values of saturation magnetization (M_s) are presented in Fig. 6. M_s increases with the proportion of magnetite and with the particle size. In average, the bigger the particle is the higher saturation magnetization of the corresponding material; the magnetite-richest Mt sample shows the highest $M_s = 70$ emu/g, which is consistent with the value reported in the literature [33] for a magnetite sample with grains of mean dimension comparable to this. Lowering the averaged particle sizes, the corresponding M_S values consistently lower.

Estimated sizes of particles, as determined from TEM images, and saturation magnetization, for coated particles only, are linearly correlate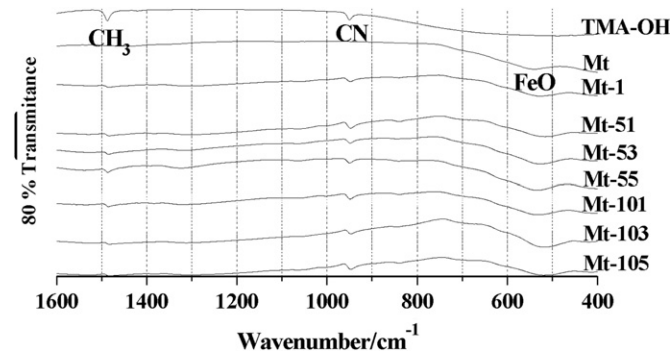d (Fig. 6). This means that a first direct effect of reducing particle sizes (ϕ) in this set of samples is lowering the corresponding saturation magnetization values, according to the following expression:

$$M_s/\mathrm{emu\,g^{-1}} = 8(2)x\phi/\mathrm{nm} + 22(9) \quad (r^2 = 0.80).$$

It is well known that crystallite size mainly depends on the balance between the nucleation and crystal growth rates [34–37]. Crystallites tend to be smaller if the nucleation rate is larger than the crystal growth rate. From elsewhere reported data, the high nucleation rate is attained by increasing the supersaturation,

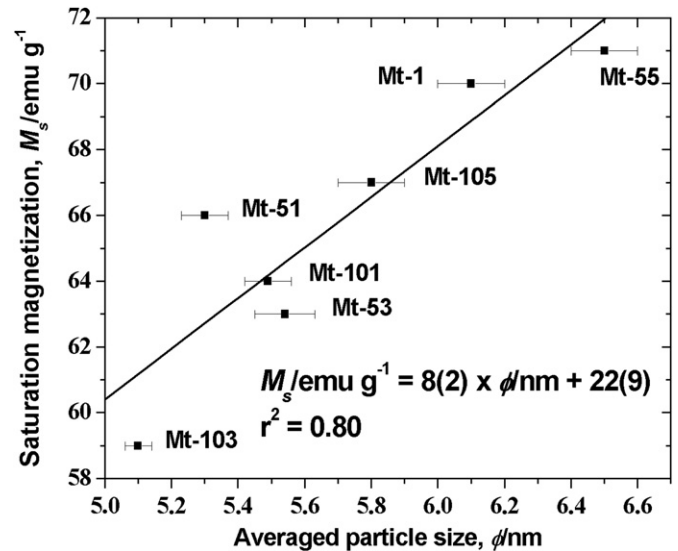**Fig. 4.** ATR-FTIR spectra of: TMA-OH, Mt, Mt1, Mt1-51, Mt1-53, Mt1-55, Mt1-101, Mt1-103, and Mt1-105,

Fig. 6. Linear dependence of the saturation magnetization ($M_s/\mathrm{emu\,g^{-1}}$) with size (ϕ/nm) of the coated particles.

Fig. 5. Hysteresis loops of: Mt, Mt1, Mt1-51, Mt1-53, Mt1-55, Mt1-101, Mt1-103, and Mt1-105.

comparatively to the growth rate, which tends to rise more sharply (or exponentially) with supersaturation [34–36]. However, these results suggest a somewhat different process. Increasing the temperature of the autoclave promotes the outer layer-dissolution of particles. The TMAOH then protects them from re-agglomerate, resulting in smaller and better-dispersed particles.

4. Conclusion

This work reports on the synthesis and preparation of magnetic monodispersed iron oxides grains with high homogeneity in size and morphology, *via* thermal treatment and use of TMAOH as dispersing chemical agent. The post-synthesis autoclave-heating promoted the decrease of the mean particle size and TMAOH tends to satisfactorily keep particles well dispersed, making the resulting primary material suitable for many technological applications as, for instance, in medical diagnosis (including contrast in magnetic resonance imagery) and therapy, due to the hyperthermic behavior of these superparamagnetic iron oxides, and for magnetically-oriented drug delivery, in oncology. Further chemical cleaning should be obviously still considered in order to effectively prepare these materials for such medical uses.

Acknowledgments

References

[1] T. Hyeon, Y. Chung, J. Park, S.S. Lee, Y.W. Kim, B.H. Park, The Journal of Physical Chemistry B 106 (2002) 6831–6833.
[2] K. Woo, H.J. Lee, J.P. Ahn, Y.S. Park, Advanced Materials 15 (2003) 1761–1764.
[3] Y. Wang, J.F. Wong, X.W. Teng, X.Z. Lin, H. Yang, Nano Letters 3 (2003) 1555–1559.
[4] A.L. Andrade, D.M. Souza, M.C. Pereira, J.D. Fabris, R.Z. Domingues, Journal of Nanoscience and Nanotechnology 9 (2009) 3695–3699.
[5] A.L. Andrade, R. Ferreira, J.D. Fabris, R.Z. Domingues (2011). Coating Nanomagnetic Particles for Biomedical Applications, Biomedical Engineering—Frontiers and Challenges, Reza Fazel (Ed.), ISBN: 978-953-307-309-5, InTech, Available from: ⟨http://www.intechopen.com/articles/show/title/coating-nano-magnetic-particles-for-biomedical-applications⟩.
[6] J.S. Bradley, B. Tesche, W. Busser, M. Masse, R.T. Reetz, Journal of the American Chemical Society 122 (2000) 4631–4636.
[7] T. Sugimoto, Y.S. Wang, Journal of Colloid and Interface Science 207 (1998) 137–149.
[8] H.T. Zhang, G. Wu, X.H. Chen, X.G. Qiu, Materials Research Bulletin 41 (2006) 495–501.
[9] D.E. Zhang, X.M. Ni, X.J. Zhang, H.G. Zheng, Journal of Magnetism and Magnetic Materials 302 (2006) 290–293.
[10] C.N.R. Rao, G.U. Kulkarni, P.J. Thomas, P.P. Edwards, Chemical Society Reviews 29 (2000) 27–35.
[11] X.H. Liu, G.Z. Qiu, X.G. Li, Nanotechnology 16 (2005) 3035–3040.
[12] A.S. Arbab, L.A. Bashaw, B.R. Miller, E.K. Jordan, B.K. Lewis, H. Kalish, J.A. Frank, Radiology 229 (2003) 838–846.
[13] P. Reimer, R. Weissleder, Radiology 36 (1996) 153–163.
[14] Q.A. Pankhurst, J. Connolly, S.K. Jones, J. Dobson, Journal of Physics D: Applied Physics 36 (2003) R167–R181.
[15] D.M. Souza, A.L. Andrade, J.D. Fabris, P. Valerio, A.M. Goes, M.F. Leite, R.Z. Domingues, Journal of Non-Crystalline Solids 354 (2008) 4894–4897.
[16] P.S. Doyle, J. Bibette, A. Bancaud, J.L. Viovy, Science 295 (2002). 2237-2237.
[17] V. Skumryev, S. Stoyanov, Y. Zhang, G. Hadjipanayis, D. Givord, J. Nogues, Nature 423 (2003) 850–853.
[18] J.I. Martin, J. Nogues, K. Liu, J.L. Vicent, I.K. Schuller, Journal of Magnetism and Magnetic Materials 256 (2003) 449–501.
[19] T. Hyeon, S.S. Lee, J. Park, Y. Chung, H. Bin Na, Journal of the American Chemical Society 123 (2001) 12798–12801.
[20] T. Sugimoto, E. Matijevic, Journal of Colloid and Interface Science 74 (1980) 227–243.
[21] Y.S. Kang, S. Risbud, J.F. Rabolt, P. Stroeve, Chemistry Materials 8 (1996) 2209–2211.
[22] J. Wang, M. Yao, G.J. Xu, P. Cui, J.T. Zhao, Materials Chemistry and Physics 113 (2009) 6–9.
[23] A.L. Andrade, D.M. Souza, M.C. Pereira, J.D. Fabris, R.Z. Domingues, Quimica Nova 33 (2010) 524–527.
[24] S.C. Qu, H.B. Yang, D.W. Ren, S.H. Kan, G.T. Zou, D.M. Li, M.H. Li, Journal of Colloid andInterface Science 215 (1999) 190–192.
[25] U. Schwertmann, R.M. Cornell, in: U. Schwertmann, R.M. Cornell (Eds.), Iron Oxides in the Laboratory: Preparation and Characterization, 1991.
[26] R.M. Cornell, The Iron Oxides: Structure, Properties, Reactions, Occurrences and Uses, ed. 2, Wiley-VCH, Weinheim, Germany, 2003.
[27] A.L. Patterson, The Scherrer formula for X-ray particle size determination, Physical Review 56 (1939) 978–982.
[28] A. Ouasri, A. Rhandour, M.C. Dhamelincourt, P. Dhamelincourt, A. Mazzah, Spectrochimica Acta Part A 58 (2002) 2779–2788.
[29] E. Barrado, F. Prieto, J. Medina, F.A. Lopez, Journal of Alloys andCompounds 335 (2002) 203–209.
[30] J.L.M. de Vidales, A. Lopez-Delgado, E. Vila, F.A. Lopez, Journal of Alloys andCompounds 287 (1999) 276–283.
[31] M. Ma, Y. Zhang, W. Yu, H.Y. Shen, H.Q. Zhang, N. Gu, Colloids and Surfaces A: Physicochemical and Engineering Aspects 212 (2003) 219–226.
[32] Y.H. Zheng, Y. Cheng, F. Bao, Y.S. Wang, Materials Research Bulletin 41 (2006) 525–529.
[33] G.F. Goya, T.S. Berquo, F.C. Fonseca, M.P. Morales, Journal of Applied Physics 94 (2003) 3520–3528.
[34] F. Di Renzo, Catalysis Today 41 (1998) 37–40.
[35] Z.A.D. Lethbridge, J.J. Williams, R.I. Walton, K.E. Evans, C.W. Smith, Microporous and Mesoporous Materials 79 (2005) 339–352.
[36] T.O. Drews, M. Tsapatsis, Current Opinion in Colloid and Interface Science 10 (2005) 233–238.
[37] S. Qiu, J. Yu, J. Zhu, O. Terasaki, Y. Nozue, W. Pang, R. Xu, Microporous and Mesoporous Materials 21 (1998) 245–251.